University of Bern

Institute for Theoretical Physics
Albert Einstein Center for Fundamental Physics

Master's Thesis

Confinement in 3-d U(1) Lattice Gauge Theory

Immanuel Albrecht

supervised by
Prof. Dr. Uwe-Jens Wiese

August 2023

Abstract

Actions for the 3-dimensional U(1) lattice gauge theory on the dual lattice in terms of height variables are derived for the vacuum case and for the case of an inserted particle-antiparticle pair. A Monte Carlo Markov chain lattice simulation for the given actions using a Metropolis algorithm is implemented. Observables such as the action, field strength, energy and correlation length are defined and simulated. Time-averaged field strength and energy density plots are shown. An estimation of the string tension of a particle-antiparticle pair is observed as the linear fit of the vacuum subtracted string potential. A second moment approach to calculate the correlation length is derived and used to plot a 1.5-step-scaling function, which shows unexpected behaviour, as the correlation length shrinks when the lattice size is increased.

Acknowledgements

I would like to thank Prof. Dr. Uwe-Jens Wiese for the opportunity to write a masters thesis about such an interesting topic that is the lattice field theory, for guidance in the exploration phase and for support in the writing process of the thesis. I am profoundly grateful for the invaluable insights granted not only during the process of writing this paper, but also during the last five years of my bachelor and master studies.

Further I would like to thank Dr. Gurtej Kanwar for helpful discussions and guidance when I was having troubles proceeding, especially the error estimation would not have been possible without his assistance.

I would also like to thank my friends and family for their continuous support. The weekly board game sessions were the refuge that allowed me to power through the work on this thesis. And without my family these studies would not have been possible to begin with.

Contents

Chapter 1

Introduction

In his seminal paper in 1974, Kenneth G. Wilson jump-started the field of lattice field theory by discretizing Abelian and non-Abelian gauge fields on a Euclidean space-time lattice, and he introduced ground-laying concepts, such as the Wilson action [1]. J. Villain iterated on the approach by approximating the Wilson action to the second order in the gauge field phase factor and he showed that this approximation preserves the correct symmetries and is in good agreement with higher order series expansions [2]. In the context of the renormalization group, the resulting Villain action is understood as a different theory in the same universality class as the Wilson action [3]. Using this result, in 1982 M. Göpfert and G. Mack showed that a 3-dimensional U(1) lattice gauge theory with Villain action shows confinement for all values of the coupling constant, and they provided a lower bound for the string tension [4]. Being well understood and simple in its description, while still experiencing effects such as confinement, makes the 3-dimensional U(1) lattice gauge theory the perfect toy example to investigate the physics of non-perturbative renormalization through lattice field theories and develop numerical methodologies such as the Monte Carlo Markov chain lattice simulations.

1.1. The scope of this thesis

In this thesis we want to investigate two key properties of the 3-dimensional U(1) lattice gauge theory: The string tension and the correlation length.

We commence by defining 3-dimensional U(1) gauge theory on a cubic lattice in analogy to [1, 2]. We then proceed to dualize the lattice field theory and define it on the dual lattice, where we find the theory to be defined in terms of integer valued variables at each site of the dual lattice, so-called height variables. The formulation of the dual theory in terms of height variables allows us to simplify numerical calculations significantly. The derived action describes the theory in a vacuum, i.e. without external charges. By inserting a Wilson loop on the original lattice, which may be interpreted as a particle-antiparticle pair being created and then later annihilated again, we find an altered action that allows us to calculate observables in the presence of charges. By stretching the Wilson loop to encompass the whole of the periodic time extent, the Wilson loop becomes a pair of Polyakov loops, representing two static charges, which we take as the basis for further investigations.

In Chapter 3 we develop a Monte Carlo Markov chain lattice simulation that is based on the action for the vacuum and Wilson loop systems we derived previously, where we utilize a Metropolis type algorithm. We also develop a cluster algorithm, which we ultimately did not use for simulation of the observables. We calculate observables including the action, the field strength, the energy, the energy density and the correlation function of the system. We produce plots of these observables, and we introduce an error estimation for the Markov chain observables by combining bootstrapping resampling with binning of consecutive observables. Finally we calculate estimates for the string tension as the linear coefficient of the vacuum subtracted string potential of the particle-antiparticle pair.

In Chapter 4 we derive a second moment approach for the calculation of the correlation length for the continuous as well as for the discrete case. We argue for the second moment approach by comparing it to the conventional least squares fit in the regime where the correlation function comes close to a parabola. We then apply the second moment method to the observed correlation functions to get correlation lengths, which then are used to extract a factor 1.5 step-scaling function. The resulting step-scaling function shows unusual behaviour, where the correlation length decreases when increasing the lattice size. The step-scaling function and the string tension are then further discussed in the conclusion of the thesis.

Chapter 2

Dualizing the 3-dimensional U(1) lattice gauge theory

2.1. Defining the 3-dimensional U(1) lattice gauge theory

Consider a 3-dimensional cubic Euclidean spacetime volume with periodic boundary conditions. We discretize the Euclidean spacetime volume on a cubic lattice with N^3 lattice sites, while respecting the periodic boundary conditions. The isotropic lattice spacing a is set to 1. We designate one dimension of the Euclidean spacetime as time, which gives us the inverse temperature of our system as the time extent of the lattice $\beta = Na$.

A U(1) gauge theory in this lattice-discretized spacetime volume has to respect certain symmetries. These are

- **Translation symmetry**: The theory should be invariant under a shift by a number of lattice spacings.
- **Gauge invariance**: The invariance under a local gauge transformation is a key feature of the theory we want to investigate.
- **Charge conjugation**: The action should be invariant under charge conjugation.
- **Parity and Time-reversal**: Reflecting either both space directions or the single Euclidean time direction around the origin should leave the action invariant.

We introduce a gauge field on the lattice by placing gauge variables $U_{xy} = e^{i\varphi_{xy}} \in U(1)$ on the links between neighbouring lattice sites $\langle xy \rangle$. A local gauge transformation takes the form

$$U'_{xy} = \Omega_x U_{xy} \Omega^*_y, \tag{2.1}$$

with $\Omega_x = e^{i\alpha_x}$, $\alpha_x \in \mathcal{R}$ being the local phase factor. The simplest non-trivial gauge invariant

term we can build on the lattice is the plaquette, a closed square of four gauge links on the lattice,

$$U'_{xy}U'_{yz}U'_{wz}{}^{*}U'_{xw}{}^{*} = U_{xy}U_{yz}U^{*}_{wz}U^{*}_{xw}. \tag{2.2}$$

This is the simplest form of a Wilson loop. While all Wilson loops are gauge invariant, we use the plaquette to construct the action for the field theory. We then proceed to construct an action from only gauge invariant terms, and the easiest way to do this is to simply sum over all plaquettes on the lattice,

$$S[U] = \frac{1}{e^2}\sum_{\square}\left(1 - \frac{1}{2}U_1U_2U_3^*U_4^* - \frac{1}{2}U_1^*U_2^*U_3U_4\right) \tag{2.3}$$

$$= \frac{1}{e^2}\sum_{\square}\left(1-\cos\varphi_{\square}\right), \tag{2.4}$$

with $\varphi_{\square} = \varphi_1+\varphi_2-\varphi_3-\varphi_4$ the sum of the phase factors of the plaquette links. Incidentally, this resembles the continuum theory term $\partial_\mu A_\nu(x) - \partial_\nu A_\mu(x)$, and the plaquette contraction is the natural object on the lattice for the field strength tensor.

The cosine term in the Wilson action (2.4) is unwieldy, as it would require us to use Bessel functions to further investigate the theory. Instead we make use of the Villain action [2],

$$S[\varphi] = \frac{1}{2e^2}\sum_{\square}\sum_{n_{\square}}(\varphi_{\square} - 2\pi n_{\square})^2, \tag{2.5}$$

where we use $n_{\square} \in \mathbb{Z}$ to get the phase factor $\varphi_{\square} \in (-\pi, \pi]$ mapped onto the real numbers; otherwise, this would be the Manton action [5]. The simple Gaussian form allows us to further simplify and later easily dualize the theory. Furthermore, the Villain action, while describing a different theory, is part of the same universality class as the Wilson action [6].

Next we want to introduce the n-form notation on the lattice, where we can relate objects associated to sites, links, plaquettes and cubes by identifying them with their respective differential forms (0-, 1-, 2- and 3-form respectively, see Figure 1). As done in [7], we introduce the exterior differential d as acting on an n-form by summing over its oriented boundary, yielding an $(n+1)$-form. For example, if we act with the exterior differential on a 1-form, which is associated to the links on the lattice, we sum up the contributions from the values on the links for each plaquette on the lattice. This gives us a 2-form, associated to the plaquettes,

$$\varphi_{\square} = d\varphi_l = \varphi_1 + \varphi_2 - \varphi_3 - \varphi_4. \tag{2.6}$$

Using this notation, we easily see that applying the exterior derivative twice vanishes,

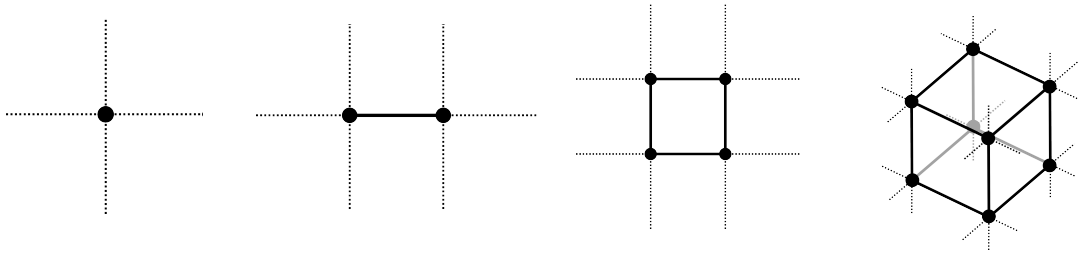

(a) 0-form (b) 1-form (c) 2-form (d) 3-form

Figure 1: The four differential forms on a 3-dimensional lattice.

$$d\varphi_\square = d^2\varphi_l = 0. \tag{2.7}$$

This is also known as the Bianchi identity. This provides a simple way to confirm gauge invariance of the plaquette again, as we simply write

$$\varphi'_\square = d(\varphi_l + d\alpha_x) = d\varphi_l + dd\alpha_x = d\varphi_l = \varphi_\square. \tag{2.8}$$

With this we finally build the partition function. On the lattice this means that we integrate over all phase factors φ_l. A key insight is that, because the phases only exist inside some periodic functions, we may decompose this integration into an integral over just one period and sum over the rest. Finally we use the Villain action [2], which yields the partition function

$$Z = \prod_l \frac{1}{2\pi} \int_{-\pi}^{\pi} d\varphi_l \prod_\square \sum_{n_\square \in \mathbb{Z}} \exp\left(-\frac{1}{2e^2}\|d\varphi_l - 2\pi n_\square\|^2\right). \tag{2.9}$$

It its to be noted that here we introduced the square of the measure of an n-form as the scalar product of the term with itself,

$$\|\varphi_\square\|^2 = (\varphi_\square, \varphi_\square) = \sum_\square \varphi_\square^2. \tag{2.10}$$

2.2. Dualizing the lattice field theory

With dualization, we intend to change the underlying mathematical structure of theories while respecting the symmetries and constraints on which they are based. For lattice theories, this is especially straightforward, as for every lattice there exists the dual lattice. In our case, a 3-dimensional cubic lattice, we define that a lattice site gets mapped onto a unit cube cell and a link between two sites gets mapped onto a plaquette. Because the dual lattice is again a 3-dimensional cubic lattice, we find that the dual of the dual lattice is again the original lattice, as it should be.

We say that each object identified as an n-form on the original lattice can also be identified as a $(3-n)$-form on the dual lattice. We denote this duality transformation with *, and this gives rise to the codifferential $\delta = {}^*d^*$, which lowers the rank of a form by 1, e.g. the codifferential of a 2-form $\chi_\square$ with dual ψ_l is a 1-form χ_l with dual $\psi_\square$,

$$\delta\chi_\square = {}^*d^*\chi_\square = {}^*d\psi_l = {}^*\psi_\square = \chi_l. \tag{2.11}$$

Note that applying the codifferential after the differential does not yield the original n-form,

$$\delta d\varphi_l = \delta\varphi_\square = \chi_l \neq \varphi_l. \tag{2.12}$$

Using the Bianchi identity (2.7), we can show that applying the codifferential twice vanishes,

$$\delta\delta = {}^*d^{**}d^* = {}^*dd^* = 0. \tag{2.13}$$

In order to dualize the lattice field theory we found in eq. (2.9), we start by using the relation

$$d\varphi_l - 2\pi n_\square = \varphi_\square - 2\pi n_\square = F_\square, \tag{2.14}$$

and we add the Bianchi identity (2.7) as a constraint. This leads to

$$Z = \prod_{\hexahedron} \delta_{2\pi}(d\varphi_\square) \prod_\square \int_{-\infty}^{\infty} dF_\square \exp\left(-\frac{1}{2e^2}\|F_\square\|^2\right), \tag{2.15}$$

where $\prod_{\hexahedron}$ is the product over all cube cells. We now may express the delta function in terms of the series expansion

$$\prod_{\hexahedron} \delta_{2\pi}(d\varphi_\square) = \prod_{\hexahedron} \sum_{k_{\hexahedron}\in\mathbb{Z}} \exp(i(k_{\hexahedron}, d\varphi_\square)) \tag{2.16}$$

$$= \prod_{\hexahedron} \sum_{k_{\hexahedron}\in\mathbb{Z}} \exp(-i(\delta k_{\hexahedron}, \varphi_\square)) \tag{2.17}$$

$$= \prod_{\hexahedron} \sum_{k_{\hexahedron}\in\mathbb{Z}} \exp(-i(\delta k_{\hexahedron}, F_\square)). \tag{2.18}$$

Here we performed a partial integration and then used periodicity. As such, the inclusion of the Bianchi identity in (2.15) yields

$$Z = \prod_{\square} \sum_{k_{\square} \in \mathbb{Z}} \exp\left(-\frac{e^2}{2}\|\delta k_{\square}\|^2\right). \tag{2.19}$$

Note that the coupling constant squared has switched from the denominator to the numerator in order to preserve dimensionality. Finally, going from the original to the dual lattice transforms the product over all cube cells into a product over all lattice sites. The integer valued variables, which we will call height variables from now on, are associated to the sites of the dual lattice, and the codifferential yields a normal exterior differential,

$$Z = \prod_{x} \sum_{h_x \in \mathbb{Z}} \exp\left(-\frac{e^2}{2}\|dh\|^2\right) \tag{2.20}$$

$$= \prod_{x} \sum_{h_x \in \mathbb{Z}} \exp\left(-\frac{e^2}{2} \sum_{\langle xy \rangle} (h_x - h_y)^2\right), \tag{2.21}$$

where $\langle xy \rangle$ refers to the sum over links—nearest neighbour pairs—on the dual lattice. This result is noteworthy, as we were able to transform a partition function in terms of the real valued variables φ_l into one that has only integer valued height variables h_x. Without having to evaluate integrals, this dualization allows for integer valued lattice simulations, simplifying Monte Carlo methods significantly.

Additionally, we observe the partition function to experience a kind of gauge symmetry, in the sense of a redundant degree of freedom, where shifting all height variables h_x up by some constant does not affect the result. This will become relevant as we investigate the system further.

The found partition function allows us to formulate, evaluate and simulate different observables, such as the energy or the mass-gap and correlation length. In a next section we will consider the insertion of charges into the theory.

2.3. Inserting charges via Polyakov loops

While the plaquette is the simplest gauge invariant construction on the lattice, we may also consider bigger Wilson loops. We find, that for Wilson loops bigger than a few plaquettes, the surface with the given Wilson loop as its boundary is not unique at all, as there exists a whole family of surfaces with the same border. Consider two surfaces S and S' with the same boundary ζ. We define surface indicator functions $\mathbb{1}_S$ and $\mathbb{1}_{S'}$ as 2-forms, that are either ± 1 for when a plaquette is part of the surface S or S' and 0 otherwise. The sign depends on the oriented boundary. The codifferential of a surface indicator function is a indicator function $\mathbb{1}_\zeta$ itself, a 1-form which is ± 1 when a link is part of the Wilson loop and 0 otherwise. Therefore, the codifferential of the indicator function of the two surfaces S and S' are equal,

$$\delta \mathbb{1}_S = \mathbb{1}_\zeta = \delta \mathbb{1}_{S'}. \tag{2.22}$$

We may transform the surfaces that have the same boundary into each other by adding to the surface indicator function $\mathbb{1}_S$ the codifferential of cube cell indicator functions $\mathbb{1}_{X^i}$, 3-forms that are ± 1 if a cube cell is the designated cube cell X and 0 otherwise,

$$\mathbb{1}_{S'} = \mathbb{1}_S + \sum_{i=1}^{N} \delta \mathbb{1}_{X^i}, \tag{2.23}$$

where $i \in \{1, 2, ..., N\}$ iterates over the required cube cells X^i to transform the surface S into S'.

With the partition function from eq. (2.9), we define a Wilson loop observable over the Wilson loop links l' as

$$\langle W_{l'} \rangle = \frac{1}{Z} \prod_l \frac{1}{2\pi} \int_{-\pi}^{\pi} d\varphi_l \prod_\square \sum_{n_\square \in \mathbb{Z}} \exp\left(-\frac{1}{2e^2} \| d\varphi_l - 2\pi n_\square \|^2 \right) \prod_{l'} \exp\left(i\varphi_{l'} \right). \tag{2.24}$$

The idea again is to dualize this expression. As we already understand how to proceed with all but the last term, lets consider some initial transformations

$$\prod_{l'} \exp\left(i\varphi_{l'} \right) = \exp\left(i \left(\mathbb{1}_{l'}, \varphi_l \right) \right) = \exp\left(i \left(\delta \mathbb{1}_S, \varphi_l \right) \right) \tag{2.25}$$

$$= \exp\left(i \left(\mathbb{1}_S, d\varphi_l \right) \right) = \exp\left(i \left(\mathbb{1}_S, \varphi_\square \right) \right) = \exp\left(i \left(\mathbb{1}_S, F_\square \right) \right). \tag{2.26}$$

Again, by inserting the Bianchi identity (2.18), we find

$$\langle W_{l'} \rangle = \frac{1}{Z} \prod_{\square\!\!\!\square} \sum_{k_{\square\!\!\!\square} \in \mathbb{Z}} \exp(-i(\delta k_{\square\!\!\!\square}, F_\square)) \prod_\square \int_{-\infty}^{\infty} dF_\square \exp\left(-\frac{1}{2e^2} \| F_\square \|^2 \right) \exp\left(i \left(\mathbb{1}_S, F_\square \right) \right) \tag{2.27}$$

$$= \frac{1}{Z} \prod_{\square\!\!\!\square} \sum_{k_{\square\!\!\!\square} \in \mathbb{Z}} \exp\left(-\frac{e^2}{2} \| \delta k_{\square\!\!\!\square} \|^2 \right) \exp\left(i \left(\mathbb{1}_S, \delta k_{\square\!\!\!\square} \right) \right) \tag{2.28}$$

$$= \frac{1}{Z} \prod_{\square\!\!\!\square} \sum_{k_{\square\!\!\!\square} \in \mathbb{Z}} \exp\left(-\frac{e^2}{2} \| \delta k_{\square\!\!\!\square} + \mathbb{1}_S \|^2 \right), \tag{2.29}$$

which is then dualized to yield

$$\langle W_{l'} \rangle = \frac{1}{Z} \prod_x \sum_{h_x \in \mathbb{Z}} \exp\left(-\frac{e^2}{2} \| dh + {}^*\mathbb{1}_S \|^2 \right), \tag{2.30}$$

where ${}^*\mathbb{1}_S$ is the indicator function whether a dual link pierces the original Wilson loop surface, and the sign depends on the orientation of the original Wilson loop. Now if we go back and consider a different surface for the given Wilson loop as in eq. (2.23), we see that it changes the height variables by a constant shift, under which the action is invariant.

Having constructed a coherent Wilson loop observable, it remains to be interpreted. As K. Wilson argued in 1974 [1], for a Wilson loop with two edges in time direction at positions x and y and two edges connecting x and y at times t and t', the resulting loop can be thought of as producing a particle-antiparticle pair at time t at the positions x and y, which exists for the duration $|t' - t|$ and then annihilates again.

In our case, because we use periodic boundary conditions, we may also construct a different case, where we stretch the Wilson loop to contain the whole extent of the time dimension. In this case, one might say that the creation and annihilation happens simultaneously, canceling each other. This results in two separate loops closed in the periodic time dimension, so-called Polyakov loops [8]. These then represent a static particle-antiparticle pair.

Finally, if we want to observe different observables in the presence of the particle-antiparticle pair, such as the energy of the string or field strength, we can utilize the adapted action

$$S[h] = \frac{e^2}{2} \| dh + {}^*\mathbb{1}_S \|^2 = \frac{e^2}{2} \sum_{<xy>} \left(h_x - h_y + {}^*\mathbb{1}_S \right)^2 . \tag{2.31}$$

Chapter 3

Lattice simulation and confinement

3.1. Simulation parameters

With the theories from Chapter 2, we are able to start performing numerical simulations to investigate the given theories further. We start by initializing a 3-dimensional cubic lattice of N^3 lattice points with periodic boundary conditions. We consider lattice sizes ranging from 16^3 to 54^3. On each lattice site x, we initialize an integer valued height variable h_x. There are two possible initialization procedures, the so-called cold or hot starts. Starting cold means to initialize all height variables to be equal, while starting hot means that we initialize the height variables as a random integer in some given range. For our purpose and going forward, we chose starting hot by initializing the height variables randomly chosen from uniformly distributed integers in the range $h_x \in [-128, 127]$. This is our first configuration $\mathcal{C}$ in the configuration space that we want to sample, the start of our Markov chain.

With the initialized system, it remains to specify certain parameters of the system: First and foremost, this is the action. Here we can choose between the two actions derived in Chapter 2. If we want to observe properties of the vacuum, we choose the action

$$S[h] = \frac{e^2}{2} \sum_{\langle xy \rangle} (h_x - h_y)^2 \,. \tag{3.1}$$

If we want to observe properties of the system in presence of two opposite static charges as seen in Section 2.3, we choose the action

$$S[h] = \frac{e^2}{2} \sum_{<xy>} (h_x - h_y + {}^*\mathbb{1}_S)^2 \,, \tag{3.2}$$

where ${}^*\mathbb{1}_S$ is the indicator function for dual links piercing the surface spanned by the two Polyakov loops on the original lattice.

We also need to specify the coupling constant e of our system. Coupling constants we consider are in the range $e^2 \in [0.4, 0.6]$, and we might choose different ranges depending on the size of the lattice and the observable we want to calculate. The chosen action and coupling constant determine the Boltzmann weight for each possible configuration of height variables, and therefore the Boltzmann distribution.

3.2. Sampling the configuration space

In order to correctly sample the configuration space of the theory, we need to produce configurations that follow the Boltzmann distribution

$$P(\mathcal{C}) = \frac{1}{Z} \exp\left(-S[\mathcal{C}]\right). \tag{3.3}$$

We achieve this by iteratively performing transformations on our initial configuration in such a way that we respect the Boltzmann weight. While there are multiple schemes to guarantee that the transformations respect the Boltzmann weight, we confirm that our transformations follow the Boltzmann distribution by showing that they obey ergodicity and the detailed balance condition. The detailed balance condition can be stated as follows: The probability of being in a state $\mathcal{C}$ and going to a state $\mathcal{C}'$ must be equal to the probability of being in the state $\mathcal{C}'$ and going back to the state $\mathcal{C}$,

$$P(\mathcal{C})P(\mathcal{C} \to \mathcal{C}') = P(\mathcal{C}')P(\mathcal{C}' \to \mathcal{C}). \tag{3.4}$$

This is reminiscent of the Bayesian theorem. Furthermore, detailed balance in combination with ergodicity ensures that the Markov chain converges to the desired stationary distribution with the transition probability depending only on the previous configuration.

Ergodicity states that the transformation must be able to reach any configuration from any other configuration in a finite number of steps. This makes sure that the entire configuration space gets sampled by the Markov chain.

3.3. Metropolis algorithm

There are many different algorithms that can be constructed with the conditions above. Here we introduce a Metropolis algorithm. Consider a configuration $\mathcal{C}$. At the position x on the lattice, the height variable has the value h_x. We then propose a new configuration $\mathcal{C}'$ that is equivalent to $\mathcal{C}$ except at x where $h'_x = h_x \pm 1$. We calculate the Boltzmann weights of both configurations

$$P(\mathcal{C}) = \frac{1}{Z} \exp\left(-S\right), \qquad P(\mathcal{C}') = \frac{1}{Z} \exp\left(-S'\right), \tag{3.5}$$

where we abbreviated $S = S[\mathcal{C}]$ and $S' = S[\mathcal{C}']$. Consider the case where S' is smaller than S, meaning that the new configuration $\mathcal{C}'$ has a higher weight than the previous. In this

case it is desirable to accept the new configuration, and we set $P(\mathcal{C} \to \mathcal{C}') = 1$. The detailed balance condition (3.4) then gives us the probability to go from a higher weight to a lower weight as

$$P(\mathcal{C}' \to \mathcal{C}) = \frac{P(\mathcal{C})}{P(\mathcal{C}')} = \exp\left(S' - S\right). \tag{3.6}$$

The case where S' is bigger than S can be calculated similarly. The full transformation probability then can be stated as

$$P(\mathcal{C} \to \mathcal{C}') = \min\{1, e^{S-S'}\}. \tag{3.7}$$

Here we note that, because we use the actions (2.5) or (2.31) from Chapter 2, the difference of the actions $S - S'$ only depends on the height values of the neighbours of x, as all other contributions cancel each other out. We exploit this in our implementation of the Metropolis algorithm.

It is obvious that this transition probability satisfies detailed balance, but what about ergodicity? If we consider any target configuration, we may construct a set of transformations such that for each point on the lattice, the height values of the original configuration get transformed into the height values of the target configuration. Because each single transformation has a non-zero probability, any target configuration is in fact reachable with a non-zero probability within a finite number of steps. Thus ergodicity is confirmed.

Now, as much as changing a single height variable is a new configuration, we did not move very far in the configuration space. Therefore we propose a transformation for each point on the lattice by choosing to move either up or down with 50 percent probability. After having accepted or denied the transformation for each point, we have completed what we call a Metropolis sweep, at which point we consider the configuration the next entry of the Markov chain.

We also developed a cluster algorithm as an alternative, however we ultimately did not use it in favour of the Metropolis algorithm. In Section 3.7 we present the cluster algorithm, show that it obeys detailed balance and ergodicity and lastly elaborate on the decision to not use it in the lattice simulation.

3.4. Thermalizing the simulation

As we start sampling the configuration space, it is unlikely that the distribution of the first hundred samples already shows a resemblance to the desired distribution, as it most probably contains configurations that have a vanishingly small Boltzmann weight. However, we are allowed to discard the first configurations, which is called the burn-in or warm-up of the Markov chain. By discarding these first outliers, we make sure that the observables we are calculating are sampled from the desired distribution, which will give us more accurate results.

To test the thermalization, we performed a lattice simulation for different lattice sizes, actions and coupling constants without burn-in. In Figure 2 we can see that for a simple observable, such as the action, the system is thermalized within around 300 Metropolis sweeps.

For the upcoming simulation and calculation of observables we use a burn-in of 2000 Metropolis sweeps. Hereby we are sure that after having thermalized the system, all subsequent configurations $\mathcal{C}^1, \mathcal{C}^2, ...$ are drawn from the desired distribution and are ready for observables to be calculated from.

3.5. Observables

With a working Markov chain of configurations $\{\mathcal{C}^j,\ j \in 1, ..., N\}$ of height variables h_x^j, we now calculate some observables. Because each calculated observable for a configuration in the Markov chain is a sample of the true distribution of the observable, averaging over all calculated observables yields the numerical approximation of the expectation value of the desired observable. The numerical approximation can be improved by a resampling procedure as described in Section 3.6, where we also estimate the error of the observable. Here we list some observables that we took interest in.

3.5.1 Action observable

Because we are required to calculate the action for each link of the lattice anyways, we might as well use it as an observable. As such we calculate for each configuration $\mathcal{C}^j$ the value

$$\langle S[\mathcal{C}^j]\rangle = \frac{e^2}{2}\sum_{\langle xy\rangle}\langle\left(h_x^j - h_y^j\right)^2\rangle. \tag{3.8}$$

Because this is one of the simpler observables we can calculate on the lattice, we use it to find the number of steps it takes to thermalize the system, as depicted in Figure 2.

3.5.2 Field strength

The field strength E is a 2-form on the original lattice, and therefore associated to the plaquettes. We distinguish the three different components of the field strength, E_x, E_y and B, by the bounding links of their plaquettes. If the plaquette has two spatial and two temporal links, then the plaquette is associated to the electric field components E_x and E_y, and we identify each of them with the direction in which the respective spatial links of their plaquettes are pointed at, e.g. the plaquette of E_x has two spatial links in x-direction. On the other hand, if the plaquette has four spatial links, then it is associated to the magnetic field component B. Dualizing the field strength yields a 1-form, where we associate each plaquette on the original lattice with the dual link piercing it,

$$E = {}^*dh. \tag{3.9}$$

In terms of the height variables, we find the field strength component E_i associated to the piercing link in i-direction for $i \in \{1, 2, 3\}$, going out from the lattice site x as

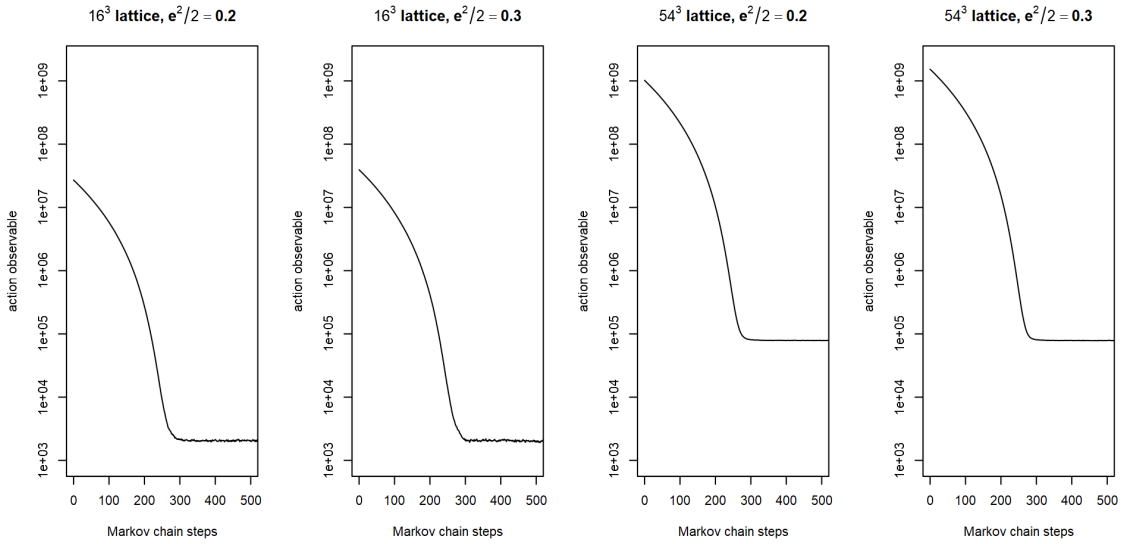

(a) Using vacuum action.

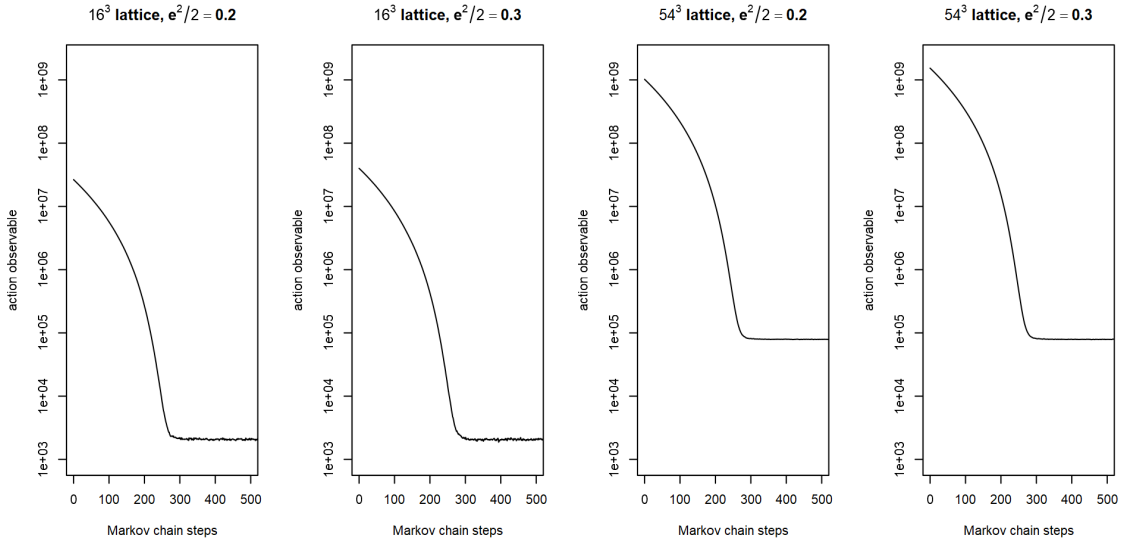

(b) Using the adapted action with an inserted particle-antiparticle pair.

Figure 2: Action observable plots with logarithmic y-axis showing thermalization behaviour for different lattice sizes and coupling constants. In 2a the vacuum action is used, and in 2b the adapted action with an inserted particle-antiparticle pair is used.

$$\langle E_{i,x}[\mathcal{C}^j]\rangle = \langle h^j_x - h^j_{x+\hat{i}}\rangle, \tag{3.10}$$

where $\hat{i}$ is a unit vector in i-direction. Tracing back the dualization, we find the field strength components as originally identified by the links of their plaquettes relate to the field strength components identified by the piercing links as

$$E_1 = E_y, \tag{3.11}$$
$$E_2 = E_x, \tag{3.12}$$
$$E_3 = B. \tag{3.13}$$

We average over all time slices of the configuration in order to plot the field strengths, as we consider only static systems when we use the vacuum action or the particle-antiparticle action. However, averaging this way is not possible for the magnetic field component, as for periodic boundary conditions the averaged magnetic field vanishes. In Figure 3 we see the time-averaged field strength plots for both electric fields and both actions for a lattice size of 16^3, and in Figure 4 we use a lattice size of 36^3. The coupling constant is held at $e^2/2 = 0.27$.

We clearly observe the sting connecting the two charges in the E_x field strength plots and we identify the opposite charges of the particle pair in the E_y field strength plots. Furthermore, we see that the fluctuations of the field strength in the vacuum case are negligible in comparison to the field strength values in presence of the particle-antiparticle pair.

3.5.3 Energy observable

Traditionally, the energy density of the electromagnetic field is given as [9]

$$u = \frac{1}{2}\left(\epsilon_0|E|^2 + \frac{1}{\mu_0}|B|^2\right). \tag{3.14}$$

However, as we are in Euclidean spacetime, we derive the energy observable as

$$\langle H[\mathcal{C}^j]\rangle = \frac{e^2}{2\beta}\left(\sum_{\langle xy\rangle \text{ spatial}} \langle (h^j_x - h^j_y)^2\rangle - \sum_{\langle xy\rangle \text{ temporal}} \langle (h^j_x - h^j_y)^2\rangle\right). \tag{3.15}$$

Here we use $\beta = Na$. The energy observable gives us a way to calculate the energy stored in the string connecting the particle-antiparticle pair, which is done in Section 3.8.

3.5.4 Energy density

The energy density for a point on the dual lattice then follows as the average over the contributions to the total energy from the incoming and outgoing dual links at the given dual lattice site,

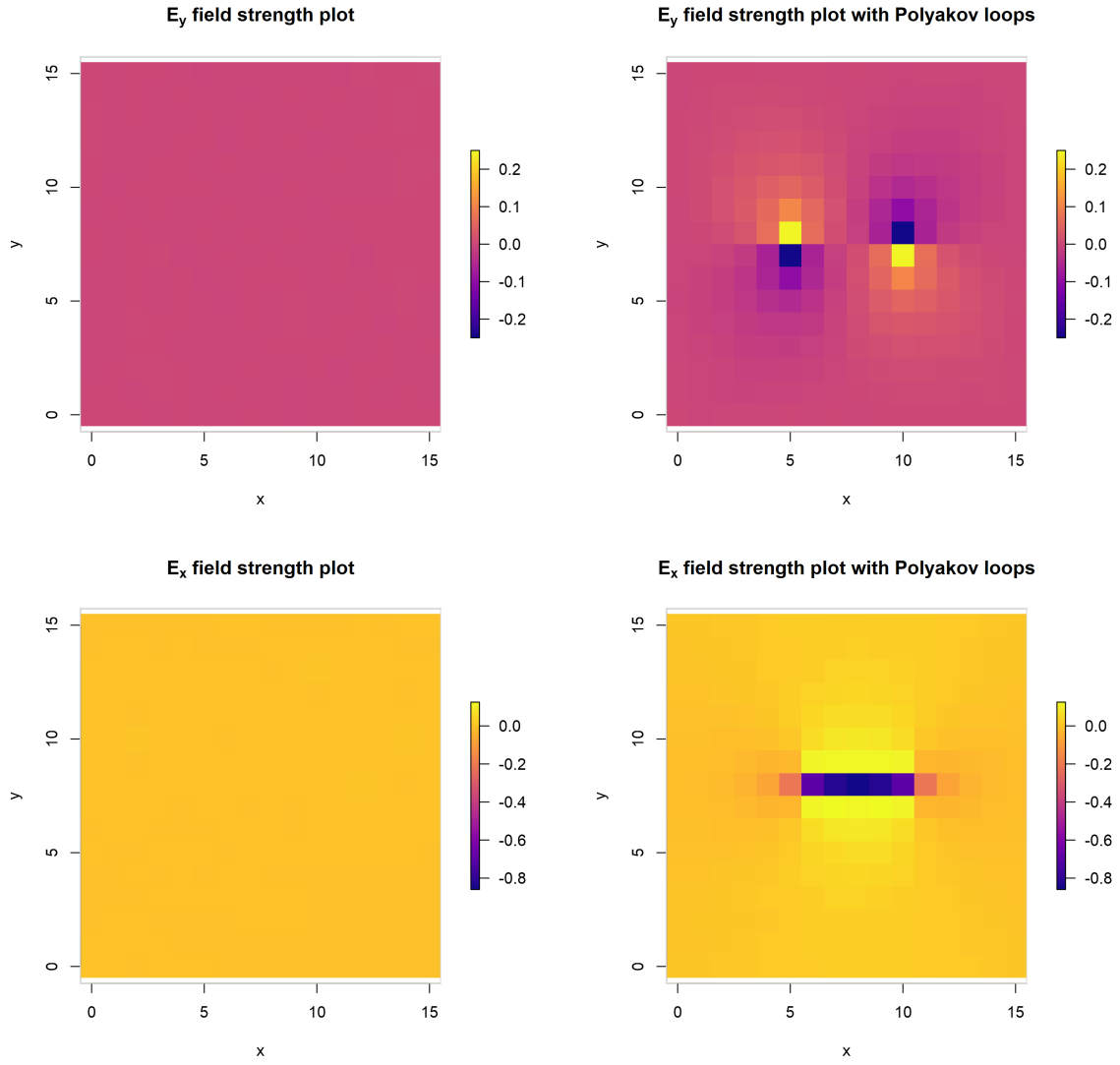

Figure 3: Time averaged field strength plots for a 16^3 lattice with and without Polyakov loops. The coupling constant is held at $e^2/2 = 0.27$.

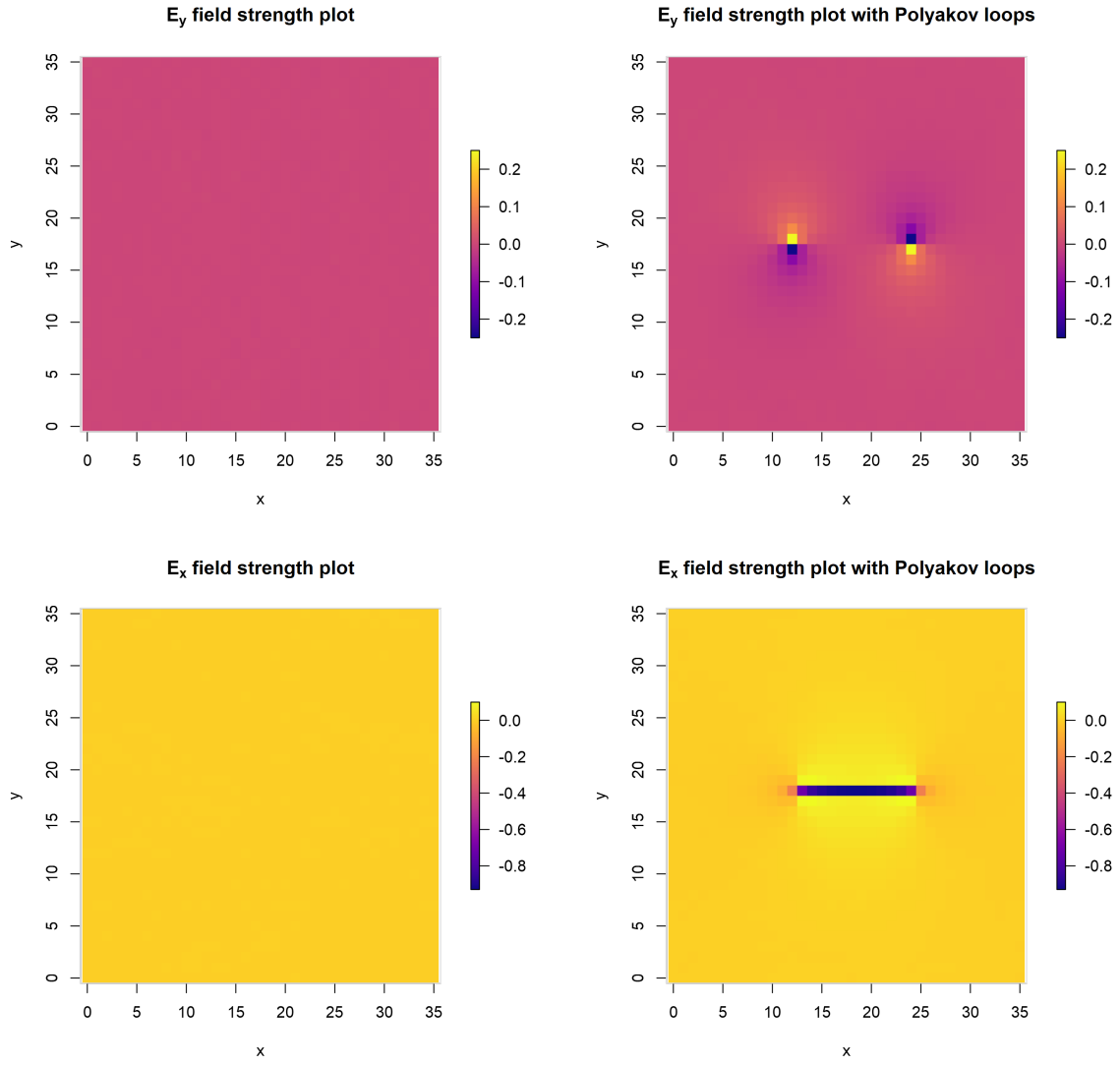

Figure 4: Time averaged field strength plots for a 36^3 lattice with and without Polyakov loops. The coupling constant is held at $e^2/2 = 0.27$.

$$\langle u(x)[\mathcal{C}^j]\rangle = \frac{e^2}{4\beta}\left(\sum_{\substack{\langle xy\rangle \text{ spatial}\\ x \text{ fixed}}} \langle (h_x^j - h_y^j)^2\rangle - \sum_{\substack{\langle xy\rangle \text{ temporal}\\ x \text{ fixed}}} \langle (h_x^j - h_y^j)^2\rangle\right) \tag{3.16}$$

As such, the energy density observable is again associated to the sites of the dual lattice, which in turn are associated to the cube cells of the original lattice. This is shown in Figure 5 for the lattice sizes 16^3 and 36^3 with a coupling constant of $e^2/2 = 0.27$.

3.5.5 Correlation function

Another observable is the correlation function. However, the implementation of the correlation function observable has some intricacies, as the naive observable $C(x-y) = \langle h_x h_y\rangle$ is not invariant under the global shift symmetry of the height variables. Instead, we use the surface width observable

$$W(x,y) = \frac{1}{2}\langle (h_x - h_y)^2\rangle, \tag{3.17}$$

and define

$$W(t) = -\frac{1}{L}\sum_{\vec{x},\vec{y},t_0} W(x=(t_0,\vec{x}), y=(t_0+t,\vec{y})) = C(t) - L\sum_x \langle h_x^2\rangle, \tag{3.18}$$

which is equivalent to the correlation function up to some constant offset. We will go into more detail about it in Chapter 4.

3.6. Error estimation

While the mean value over the Markov chain observables is a good starting point for our analysis, we will sooner than later require an error estimation for the observables. This error estimation is non-trivial, as consecutive configurations in the Markov chain can be highly correlated, depending on the algorithm. Luckily, the bootstrapping procedure with binning is able to take this correlation into account.

3.6.1 Bootstrapping resampling

If we assume that the data collected from our numerical experiment, in our case that would be the configurations of our Markov chain, is representative of the total population, then we are allowed to use bootstrapping resampling to improve our observations and estimate their errors. This works as follows:

First we build the resampled ensembles. We decide on an number of ensembles we want to create. For a quick data analysis this is usually 100 ensembles, for the final analysis it is 1000. For each ensemble we draw data points from our original data with replacement and add them to the resampled ensemble until we have the same number of data points as there

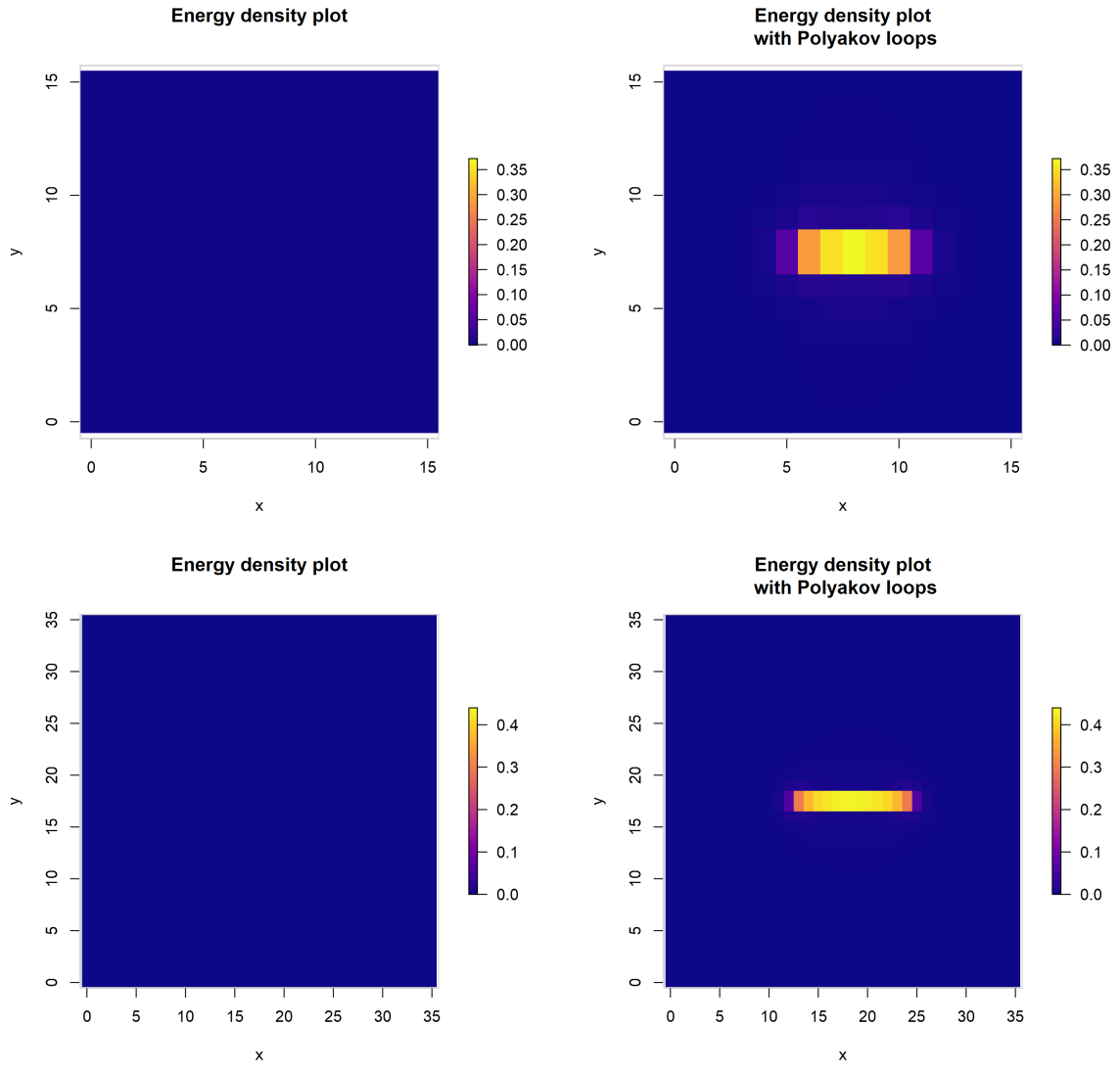

Figure 5: Time averaged energy density plots for lattices of size 16^3 and 36^3 with coupling constant $e^2/2 = 0.27$.

are in the original data set. Note that by drawing with replacement, the resampled ensemble has a very high likelihood to contain duplicates of the same data points while leaving out others.

After having built the resampled ensembles, we perform the same analysis on the resampled data set as we did on the original. This means in our case that for each resampled Markov chain we calculate the observables and calculate the expectation value as the mean over the observables of the whole Markov chain. This results in an expectation value for each resampled ensemble, which again is a distribution of values, and on which we may again perform a statistical analysis. The average over all expectation values can in this case be considered our estimation of the true expectation value, and the standard deviation then is our estimation of its true error.

For a pictorial representation of the bootstrapping procedure consider Figure 6.

3.6.2 Binning

While bootstrapping allows us to estimate the true error of our observable, it doesn't yet take into account the correlation between consecutive configurations in the Markov chain, and therefore underestimates the error of the observables. This can be alleviated by considering some groups of consecutive configurations as inherently linked and building groups. Such a group of consecutive configurations is called a bin, and the number of data points in one bin we call the bin size. As such, during the resampling procedure, we don't choose single data points to add to the resampled ensemble, but instead we draw from the collection of bins with replacement and add all points inside the drawn bin to the ensemble, until the number of data points in the resampled ensemble matches the number in the original data set. Optimally, the number of data points is divisible by the bin size.

Binning should increase the estimated error of the observables, as they were previously underestimated. Starting from a bin size of 1 data point, the error grows with increasing bin size until at some point this growth slows down and levels off. If the bin size becomes too large, with the number of data points being only a small factor larger than the bin size, the error starts to vary wildly, becoming zero when the bin size is equal to the number of data points. We thus aim to stop the binning when the error levels off, at which point the error estimation is considered to take the correlation into account.

There are minor differences between the binned bootstrapping procedure and the block bootstrapping as found in [6]. Where we group the data into bins, the block bootstrapping adds a number of consecutive data points to the resampled ensemble whenever it draws with replacement data points from the original data set. This approach increases the permutations of possible resampled ensembles and as such produces generally smaller error estimates. Furthermore, there is the jackknife bootstrapping procedure, which repeatedly calculates the statistics of the data collection with a single data point removed [10]. The jackknife procedure is the least computationally expensive of the procedures discussed, although it is limited in its applicability for different statistics such as the median. We stick to bootstrapping resampling with binning.

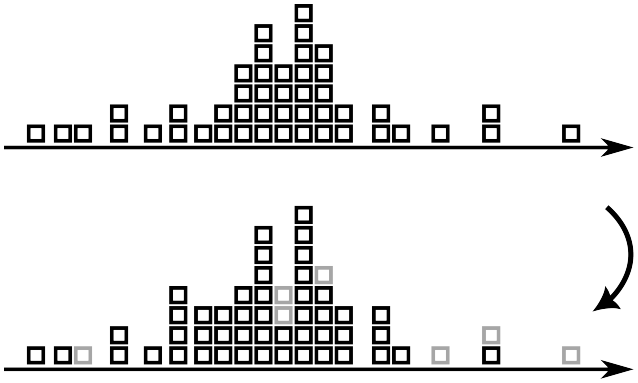

(a) From our original data set we draw observations with replacement to build one of the resampled ensembles. Some data points are repeated while others are left out.

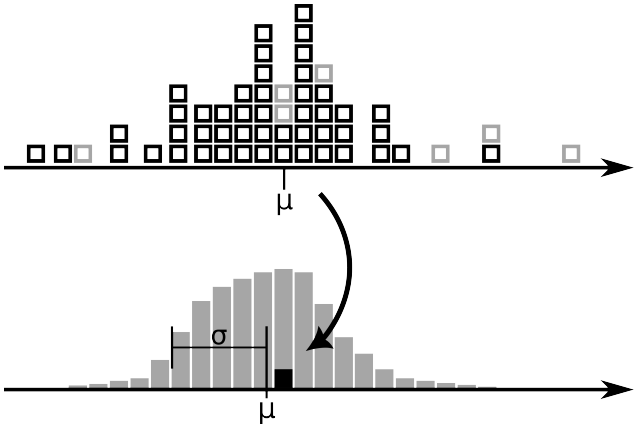

(b) The resampled ensemble provides a sample of the observable. Repeating the resampling yields a distribution, from which the mean gives an estimation of the true observable, while the standard deviation is the estimated error.

Figure 6: The bootstrapping procedure

3.6.3 Parallelization

We considered two options to employ parallel computing for lattice simulations. We could either choose an algorithm that allows for multiple changes to be done in parallel on the configurations of the Markov chain, such as dividing up the lattice in a checkerboard manner in even and odd sites and then performing a Metropolis sweep on only the even or odd sites respectively, such that the parallel operations don't interfere with each other, or we could simply perform multiple lattice simulations in parallel and then combine the results. For simplicity's sake we chose the latter, although combining the results of simulations with the same parameters is not quite straightforward.

While we combat the correlation of consecutive configurations inside the same Markov chain by binning data points, this is not necessary when combining the data of uncorrelated simulations with the same simulation parameters. Thus we modify the bootstrapping procedure. For each resampled ensemble we want to build, we first resample the collection of simulations by choosing simulations with replacement and readying them to be resampled until we have the same number of simulations ready. Thus there might be multiple copies of the same simulation present. We then perform the usual binning and resampling for each readied simulation. We combine all these resampled simulations to build one resampled ensemble, for which the usual analysis is then performed.

3.7. Cluster algorithm

In this section we present an alternative to the Metropolis algorithm introduced in Section 3.3, the cluster algorithm. The goal is again to produce a transformation of one height variable configuration to the next, respecting detailed balance (3.4) and ergodicity. The key idea of the cluster algorithm is to group the height variables into clusters, and transform the group as a whole.

We commence by choosing a mirror plane as a value within the range of height values. We accomplish this by picking a site x on the lattice, whose height variable h_x from the previous configuration gives us the mirror plane height value. We then may shift the mirror plane up or down by a half integer $\epsilon \in \{-\frac{1}{2}, 0, \frac{1}{2}\}$. This gives us the final mirror plane height value $h = h_x + \epsilon$.

The next step is to build clusters of adjacent height variables. Consider a pair of neighbouring height variables h_x and h_y. We want to figure out whether the two height variables should be grouped for the transformation. For one, we never want to group height variables on opposite sides of the mirror plane. It follows that we also never connect to values on the plane itself, as this might indirectly connect height variables on opposite sides. If we reflect the height variable h_x at the mirror plane, this gives $h'_x = 2h - h_x$. If the two height variables were on the same side of the mirror plane, reflecting just one will increase their difference and thus the action, which in turn decreases the Boltzmann weight. In this case we want to reflect the height variables together. To add the two height variables to the same cluster, we activate the link connecting the two with a probability of

$$P_{\text{bond}} = 1 - \frac{e^{-S'}}{e^{-S}} = 1 - \frac{e^{-\frac{e^2}{2}(h'_x - h_y)^2}}{e^{-\frac{e^2}{2}(h_x - h_y)^2}}, \tag{3.19}$$

where S is the action of the single bond connecting the two height variables and S' is the action if one of the two height variables would be reflected at the mirror plane. With this choice of probability no height variables on opposite sides or in the mirror plane will be connected to each other.

In a last step, for each cluster of height variables we choose to either reflect or not reflect the whole cluster around the mirror plane with a 50 percent probability. This then generates a new configuration for the Markov chain.

We can quite elegantly show detailed balance by considering the probability of not setting a bond. The probability of not setting a bond in the case S' of opposite sides is equal to 1, while we have $1 - P_{\text{bond}}$ for the case S. Then

$$e^{-S'}1 = (1 - P_{\text{bond}})e^{-S} \Leftrightarrow P_{\text{bond}} = 1 - \frac{e^{-S'}}{e^{-S}}. \tag{3.20}$$

At last, ergodicity can be considered fulfilled, as one might imagine any configuration reachable by an finite iterative process where we always have a non-zero probability to get the right transformation. A more formal proof is omitted here.

The cluster algorithm has a few advantages. In comparison to the Metropolis algorithm, the cluster algorithm does not have a rejection step, and will always generate a new configuration. Where the Metropolis algorithm only moves a height variable one up or down at the time, the cluster algorithm makes big steps inside the configuration space. Also, the cluster algorithm might be less affected by critical slowing down, although we did not investigate this further.

However, we did not use the cluster algorithm in the end. Where the Metropolis algorithm is easily adaptable to the case with inserted Polyakov loops, this is not the case for the cluster algorithm. Flipping a cluster, where some of the activated bonds pierce the oriented surface of the Wilson loop, reverses the oriented surface as well. This and some numerical considerations discouraged us from using the cluster algorithm.

3.8. String potential

With the energy observable (3.15) we are able to construct the string tension by subtracting the vacuum energy from the energy in a system with an inserted particle-antiparticle pair. The observed potential, dependent on the distance r of the two charges, then can be fitted as

$$V(r) = const. + \sigma r + \frac{\gamma}{r} + \mathcal{O}(\frac{1}{r^2}), \tag{3.21}$$

where σ defines the string tension and γ is a universal factor depending on the dimensions of the system [11, 12]. The vacuum subtracted string potential for $e^2/2 = 0.26$ is illustrated in Figure 7.

3.8.1 String tension

By simply fitting the found potentials, we obtain a first estimate of the string tension. The string tension is not dependent on the size of the lattice, and as we calculate the slope of the string potential for bigger and bigger lattices, we would get closer to the string tension. This is done in Figure 8. We can see a tendency for a steeper slope for bigger lattice sizes, although this is less evident for larger coupling constants. Here we would require more data on even larger lattices to make a conclusive statement.

Furthermore, we can see that the observed string potential slopes all agree with the lower bound of the string potential as laid out by Göpfert and Mack [4],

$$\sigma \geq C \cdot \beta^{-1/2} a^{3/2} \exp(-\beta C(0)/2), \tag{3.22}$$

where $0 < C < 1$ is an arbitrary constant, $\beta = 4\pi^2/e^2$, a is the lattice spacing and $C(0) \approx 0.2527$. Evaluating this expression with $C = 1$ for the coupling constants $e^2/2 \in [0.2, 0.3]$ yields values between $3.8 \cdot 10^{-7}$ and $2.2 \cdot 10^{-5}$, four orders of magnitude smaller than the observed slopes.

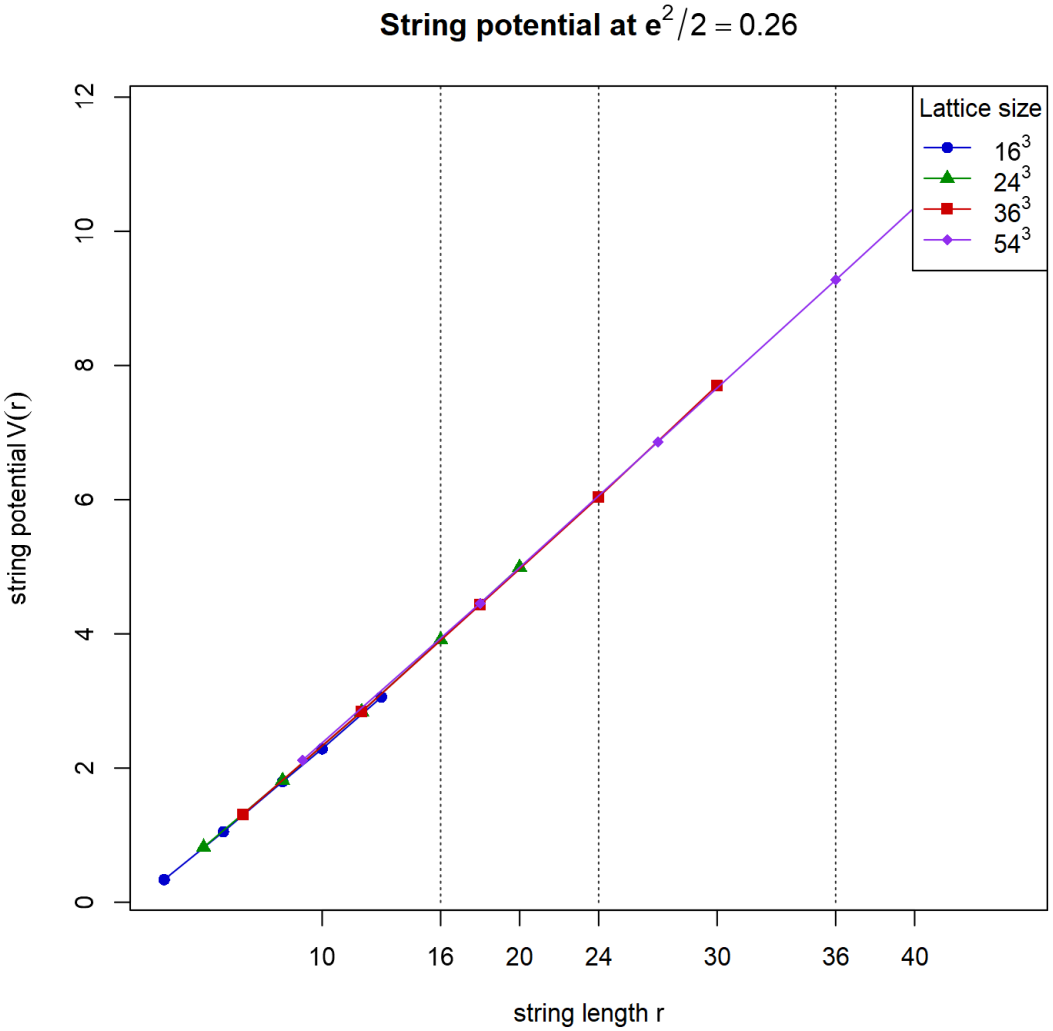

Figure 7: Vacuum subtracted string potentials for different lattice sizes for the coupling constant $e^2/2 = 0.26$.

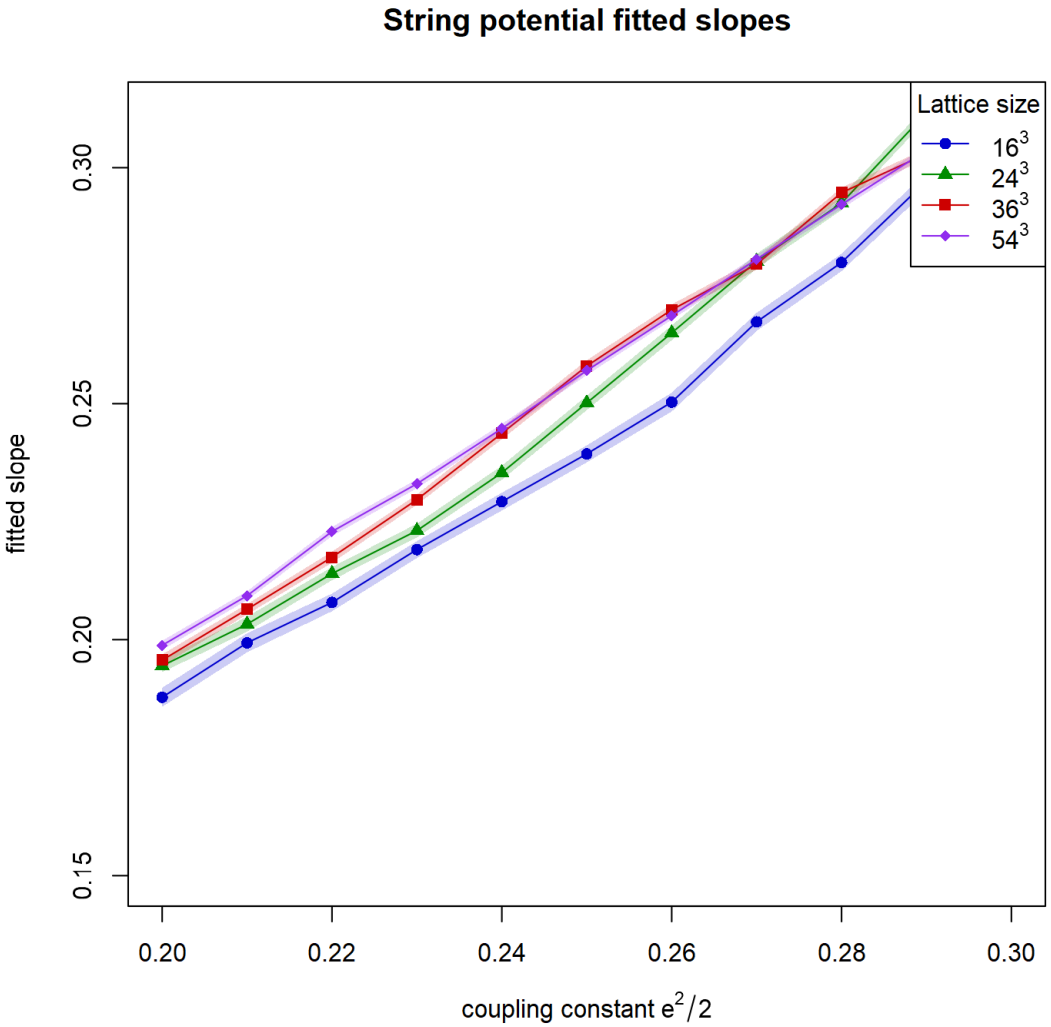

Figure 8: Fitted slopes for given coupling constants and lattice sizes with connecting lines to guide the eye.

Chapter 4

Correlation length and step-scaling function

4.1. Deriving the correlation function

In order to extract the correlation length from the Monte Carlo Markov chain simulation, we need to establish a correlation function observable. Because the observable needs to respect the symmetries of the system, the simple function

$$C(x-y) = \langle h_x h_y \rangle, \tag{4.1}$$

where h_x and h_y are height variables at the sites x and y, is not a candidate as it is not invariant under the global shift of the height variables. Instead we follow [13] and consider the surface width observable

$$W(x,y) = \frac{1}{2}\langle (h_x - h_y)^2 \rangle. \tag{4.2}$$

Obviously this observable has the required invariance under a global shift in the height variables. In order to respect periodicity of the lattice, we average over all lattice sites. We define

$$W(t) = -\frac{1}{L}\sum_{\vec{x},\vec{y},t_0} W(x=(t_0,\vec{x}), y=(t_0+t,\vec{y})) \tag{4.3}$$

$$= \frac{1}{L}\sum_{\vec{x},\vec{y},t_0} \left(\langle h_x h_y \rangle - \langle h_x^2 \rangle\right) \tag{4.4}$$

$$= C(t) - L\sum_{x}\langle h_x^2 \rangle. \tag{4.5}$$

We see that by using the surface width observable, we can extract the correlation length from eq. (4.1), although with a constant offset. This additional offset changes the zero-momentum mode, but leaves the non-zero modes unaffected. We will make use of this fact by calculating an adapted version of the second moment correlation length, which originally related the zero mode to the first non-zero mode in order to calculate the mass gap, but our adapted version will work for any momentum mode.

Some of the correlation functions are illustrated in Figure 10.

4.2. Second moment correlation length

In order to extract the correlation length from a correlation function, the standard approach is to make a fit of the correlation function in order to extract the asymptotic behaviour. However, the additional offset from the derivation above would require an additional parameter to be fitted, which would destabilize our results. We therefore take a different approach by making use of the second moment correlation length.

Due to the periodic boundary conditions, the correlation function takes the shape of a linear combination of hyperbolic cosine functions and an offset. By considering the low momentum modes of the momentum decomposition, we may nonetheless extract the mass gap and in turn the true correlation length. We make the ansatz

$$g(x) = A\cosh(m(x - \beta/2)), \tag{4.6}$$

where β is the time extent of the lattice and m models the asymptotic behavior—the mass gap.

With the goal of convincing ourselves of the validity of the second moment approach, we will first look at the continuous time case and check if the second moment approach yields the desired result. Afterwards, we will consider the discrete time case, where we check that the continuum limit of vanishing lattice spacing coincides with the results of the continuum case calculations.

4.2.1 Continuous time case

In the continuous case, the decomposition of the correlation function is given as

$$G(p) = A\int_0^\beta dx g(x)e^{ipx}. \tag{4.7}$$

By evaluating this integral with the ansatz from eq. (4.6), we find

$$G(p) = \frac{A}{2}\left[e^{-m\beta/2}\frac{e^{\beta(m+ip)} - 1}{m + ip} + e^{m\beta/2}\frac{e^{\beta(-m+ip)} - 1}{-m + ip}\right]. \tag{4.8}$$

Although we will not be using the zero mode in the final version, here we want to use it to test the original definition of the second moment correlation length.

$$G(0) = \frac{2A}{m} \sinh(m\beta/2). \tag{4.9}$$

The next-higher momentum is $p_1 = 2\pi/\beta$, but here we will generalize to arbitrary multiples $p_n = 2\pi n/\beta$. Inserting these momenta into (4.8), we find

$$G(p_n = \frac{2\pi n}{\beta}) = \frac{2A}{m} \sinh(m\beta/2) \frac{m^2}{m^2 + p_n^2}, \tag{4.10}$$

which, for $n = 0$, yields the zero mode as seen above.

The original definition of the second moment correlation length, as found in [14], is

$$\xi_{\text{2nd}} = \frac{1}{p_1} \sqrt{\frac{G(0)}{G(p_1)} - 1}. \tag{4.11}$$

Inserting the eqs. (4.9) and (4.10) for $n = 1$ gives the desired result

$$\frac{1}{p_1} \sqrt{\frac{G(0)}{G(p_1)} - 1} = \frac{1}{p_1} \sqrt{\frac{m^2 + p_1^2}{m^2} - 1} = \frac{\beta}{2\pi} \sqrt{\frac{4\pi^2}{m^2\beta^2}} = \frac{1}{m} = \xi. \tag{4.12}$$

The next step is to modify and generalize the original second moment correlation length (4.11) to accept arbitrary momenta. We therefore propose the formula

$$\xi_n = \frac{1}{p_1} \sqrt{\frac{G(p_n)/G(p_{n+1}) - 1}{(n+1)^2 - n^2 G(p_n)/G(p_{n+1})}}. \tag{4.13}$$

We can see that for $n = 0$ our proposal reduces to the original correlation length in eq. (4.1). Further, the alternative correlation length definition given in [13] states

$$\xi_b = \frac{1}{p_1} \sqrt{\frac{G(p_1)/G(p_2) - 1}{4 - G(p_1)/G(p_2)}}, \tag{4.14}$$

which fits our proposal for $n = 1$. Finally, we verify our proposal by inserting the two modes for p_n and p_{n+1} from eq. (4.10) into the formula (4.13). Because the modes only appear in the form $G(p_n)/G(p_{n+1})$, we calculate

$$G(p_n)/G(p_{n+1}) = \frac{m^2 + p_{n+1}^2}{m^2 + p_n^2}, \tag{4.15}$$

from which follows

$$G(p_n)/G(p_{n+1}) - 1 = (2n+1)\frac{1}{n^2}\frac{1}{m^2\beta^2/4\pi^2n^2 + 1}, \tag{4.16}$$

and

$$(n+1)^2 - n^2 G(p_n)/G(p_{n+1}) = (2n+1)\frac{m^2\beta^2/4\pi^2n^2}{m^2\beta^2/4\pi^2n^2 + 1}. \tag{4.17}$$

These equations then give us very nicely

$$\frac{1}{p_1}\sqrt{\frac{G(p_n)/G(p_{n+1}) - 1}{(n+1)^2 - n^2 G(p_n)/G(p_{n+1})}} = \frac{\beta}{2\pi}\sqrt{\frac{4\pi^2}{m^2\beta^2}} = \frac{1}{m} = \xi \tag{4.18}$$

This verifies the generalized second moment correlation length formula.

4.2.2 Discrete time case

Now, although this is a very pretty result, in our application we consider discrete time correlation functions with the number of data points ranging in the few dozens, so we cannot assume that the second moment correlation length formula is applicable here. Instead we construct a new second moment correlation length formula for the discrete time case. Consider again the ansatz

$$g(x) = A\cosh(m(x - \beta/2)). \tag{4.19}$$

Where previously x was a continuous variable, now we only have $N = \beta/a$ points of the correlation function at $x_j = aj$, where $j \in \{0, ..., N-1\}$ and a is the lattice spacing in the time direction (usually assumed to be 1). We label the values of the correlation function as $g_j = g(x_j)$. In order to extract the correlation length using the non-zero momenta, we perform a discrete Fourier transform

$$G_n = a\sum_{j=0}^{N-1} g_j e^{ip_n x_j}, \tag{4.20}$$

where G_n is the Fourier transform of g_j and $p_n = 2\pi/\beta$ the momentum associated to the Fourier mode. The factor a was added as an amplitude to preserve the continuum limit. Because g_j is real-valued, its Fourier transform satisfies the equality

$$G_n = G^*_{N-n}, \tag{4.21}$$

meaning the real part of the Fourier transform is symmetric and the imaginary part is anti-symmetric around $N/2$. Calculating the Fourier transform for the ansatz $g_j = A\cosh(m(x_j - \beta/2))$ gives

$$G_n = aA\frac{\sinh(m\beta/2)\sinh(ma)}{\cosh(ma) - \cos(p_n a)}. \tag{4.22}$$

We can extract the m parameter by building a quotient and rearranging. We see that

$$\frac{G_n}{G_m} = \frac{\cosh(ma) - \cos(p_m a)}{\cosh(ma) - \cos(p_n a)}. \tag{4.23}$$

This reduces to

$$\cosh(ma) = \frac{G_n\cos(p_n a) - G_m\cos(p_m a)}{G_n - G_m}, \tag{4.24}$$

which we label the second moment correlation length formula for momenta p_n and p_m. We also may recover the continuous time case. Using eq. (4.24) and expanding to the second term yields

$$1 + \frac{a^2}{2\xi^2} = 1 - \frac{a^2}{2}\frac{G_n p_n^2 - G_m p_m^2}{G_n - G_m}, \tag{4.25}$$

where we also expanded the cosine terms. Solving for ξ we find

$$\xi = \frac{\beta}{2\pi}\sqrt{\frac{G_n - G_m}{m^2 G_m - n^2 G_n}} = \frac{\beta}{2\pi}\sqrt{\frac{G_n/G_m - 1}{m^2 - n^2 G_n/G_m}}, \tag{4.26}$$

which for $m = n + 1$ is the formula (4.13) we derived for the continuous time case.

4.3. The second moment advantage and limitations

In employing the second moment correlation length, we gain the advantage of not having to rely on a least squares fit of the correlation function to extract the correlation length. This benefits us twofold.

For one, where the second moment method is the simple application of a formula, the least squares model function is fundamentally a nonlinear problem, requiring the use of numerical methods to approximate the real fit parameters up to a given accuracy. This can be

considered a black box process, and while statistical methods are still applicable for the least squares regression, it is more straightforward to do the error calculation for the second moment approach.

The second advantage is that the second moment method is able to ignore the constant offset (zero mode) of the correlation function, the least squares regression is required to take the offset into account to produce the fit. This very much interferes with the quality of the produced correlation length estimate for longer correlation lengths, which we demonstrate in the following calculations:

Assuming we want to fit the function $f(x) = A\cosh((x-\beta/2)/\xi) - A$ with values for $x \in [0, \beta]$. Then

$$f(0) = A\cosh(-\frac{\beta}{2\xi}) - A = \frac{A\beta^2}{4\xi^2}(1 + \frac{\beta^2}{12\xi^2}) + \mathcal{O}((1/\xi)^6). \tag{4.27}$$

As the correlation length increases, the correlation between the fitted amplitude A and the squared mass term m^2 increases as well, until the hyperbolic cosine becomes indistinguishable from a parabola, at which point they become totally correlated, and no meaningful fit can be calculated. Assuming that we can still detect the contributions of $1/\xi^4$ terms if they are around $1/12$ of the $1/\xi^2$ term, this gives us an upper bound on the correctly identifiable correlation length of

$$\frac{1}{12} \leq \frac{\beta^2}{12\xi^2} \Leftrightarrow \xi \leq \beta. \tag{4.28}$$

What happens if the hyperbolic cosine becomes a parabola in the second moment approach? Consider approximating the ansatz (4.6) to order $1/\xi^2$. We ignore the amplitude, as it gets canceled in the second moment approach. This gives

$$G(p_n) \simeq \int_0^\beta dx \left(1 + \frac{(x-\beta/2)^2}{2\xi^2}\right) e^{ip_n x} \tag{4.29}$$

$$= e^{ip_n\beta/2} \int_{-\beta/2}^{\beta/2} dx \left(1 + \frac{x^2}{2\xi^2}\right) (\cos(p_n x) + i\sin(p_n x)). \tag{4.30}$$

As this is a symmetric integral, the sine integral vanishes. We also use $p_n = 2\pi n/\beta$, and obtain

$$G(p_n) \simeq e^{i\pi n} \int_{-\beta/2}^{\beta/2} dx \left(1 + \frac{x^2}{2\xi^2}\right) \cos(2\pi n x/\beta) \tag{4.31}$$

$$= (-1)^n \frac{\beta}{2\pi} \int_{-\pi}^{\pi} dx \left(1 + \frac{\beta^2 x^2}{8\pi^2\xi^2}\right) \cos(nx) \tag{4.32}$$

$$= (-1)^n \frac{\beta^3}{4\pi^2\xi^2 n^2} \cos(\pi n) = \frac{\beta^3}{4\pi^2\xi^2 n^2}. \tag{4.33}$$

Up to order $1/\xi^2$ the ratio of the two Fourier transforms cancels all but the mode dependence

$$G(p_n)/G(p_m) \simeq \frac{m^2}{n^2}. \tag{4.34}$$

If we were to insert this ratio into the second moment correlation length formula (4.13), then the correlation length would diverge, as the quotient inside the square root is undefined. As such we cannot observe the correlation length with the second moment approach when the correlation function becomes a parabola. We proceed to order $1/\xi^4$, and we find

$$G(p_n) \simeq \int_0^{\beta} dx \left(1 + \frac{(x-\beta/2)^2}{2\xi^2} + \frac{(x-\beta/2)^4}{24\xi^4}\right) e^{ip_n x} \tag{4.35}$$

$$= e^{ip_n\beta/2} \int_{-\beta/2}^{\beta/2} dx \left(1 + \frac{x^2}{2\xi^2} + \frac{x^4}{24\xi^4}\right) \cos(p_n x) \tag{4.36}$$

$$= \frac{\beta^3}{4\pi^2\xi^2 n^2} + (-1)^n \frac{\beta}{2\pi} \int_{-\pi}^{\pi} dx \frac{\beta^4 x^4}{384\pi^4\xi^4} \cos nx \tag{4.37}$$

$$= \frac{\beta^3}{4\pi^2\xi^2 n^2} + \frac{\beta^5}{96\pi^4\xi^4 n^2} \left(\pi^2 - \frac{6}{n^2}\right) \tag{4.38}$$

$$= \frac{\beta^3}{4\pi^2\xi^2 n^2} \left(1 + \frac{\beta^2}{24\pi^2\xi^2} \left(\pi^2 - \frac{6}{n^2}\right)\right). \tag{4.39}$$

The ratio yields

$$G(p_n)/G(p_m) \simeq \frac{m^2}{n^2} \frac{1 + \frac{\pi^2 - 6/n^2}{24\pi^2} \left(\frac{\beta}{\xi}\right)^2}{1 + \frac{\pi^2 - 6/m^2}{24\pi^2} \left(\frac{\beta}{\xi}\right)^2}. \tag{4.40}$$

Expanding in β/ξ we get

$$G(p_n)/G(p_m) \simeq \frac{m^2}{n^2}\left(1+\frac{\pi^2-6/n^2}{24\pi^2}\left(\frac{\beta}{\xi}\right)^2-\frac{\pi^2-6/m^2}{24\pi^2}\left(\frac{\beta}{\xi}\right)^2\right) \tag{4.41}$$

$$= \frac{m^2}{n^2}\left(1+\frac{\beta^2}{4\pi^2\xi^2}\left(-\frac{1}{n^2}+\frac{1}{m^2}\right)\right) \tag{4.42}$$

For our usual choice of $n = 1$ and $m = 2$ this means

$$G(p_1)/G(p_2) \simeq 4\left(1-\frac{3\beta^2}{16\pi^2\xi^2}\right) = 4-\frac{3\beta^2}{4\pi^2\xi^2} \tag{4.43}$$

Inserting into the second moment correlation length formula (4.13) gives

$$\xi_{12} = \frac{\beta}{2\pi}\sqrt{\frac{G(p_1)/G(p_2)-1}{4-G(p_1)/G(p_2)}} \tag{4.44}$$

$$= \frac{\beta}{2\pi}\sqrt{\frac{4\pi^2\xi^2}{3\beta^2}\left(3-\frac{3\beta^2}{4\pi^2\xi^2}\right)} \tag{4.45}$$

$$= \frac{\beta}{2\pi}\sqrt{\frac{4\pi^2\xi^2}{\beta^2}-1} \tag{4.46}$$

$$= \xi\sqrt{1-\frac{\beta^2}{4\pi^2\xi^2}} \tag{4.47}$$

As such, where the second moment correlation length previously diverged, now the second moment method is able to observe all correlation lengths $\xi \geq \beta/2\pi$ with a maximal difference to the real correlation length of

$$\max|\xi-\xi_{12}| = \beta/2\pi. \tag{4.48}$$

However, this difference is not observable, because at correlation lengths of less than half the lattice spacing we observe correlation functions that allow for measurements beyond the term of order $1/\xi^4$, or the correlation lengths become too short and the correlation functions become mostly noise. We also want to consider different momentum modes. Solving the calculation above for the general case $m = n + 1$ yields

$$\xi_{n,n+1} = \xi\sqrt{1-\frac{\beta^2}{4\pi^2n^2\xi^2}} \tag{4.49}$$

4.4. Measuring correlation functions and correlation lengths

In order to determine different correlation lengths, we first have to measure the correlation functions. We do this by producing correlation functions as described in the Sections 3.5 and 4.1. We employed the binning and bootstrapping procedure that we introduced in Section 3.6 to estimate the true expectation value and the error of each value of the correlation function. Some of the correlation functions we used to calculate the correlation lengths and later the step-scaling function are illustrated in Figure 10. These are highly usable as we employed high statistics to produce a good quality result for the correlation length analysis and for the step-scaling function.

In the case where the coupling constant is too small and the correlation function comes close to a parabola, the second moment approach becomes unstable as previously discussed, and requires even higher statistics to derive a usable result. On the other hand, for very short correlation lengths, found for larger coupling constants, the correlation functions become mostly noise and are therefore not usable for the second moment approach. Such correlation functions are shown in Figure 9.

Next we calculate the correlation lengths from the usable correlation functions again via binning and resampling for different lattice sizes and coupling constants. The calculated second moment correlation lengths are shown in Figure 11. We observe a trend that for smaller lattice sizes the correlation lengths get overestimated for decreasing coupling constant $e^2/2$. This is further investigated in the next section with the use of a step-scaling function.

4.5. The step-scaling function

The step-scaling function as introduced by M. Lüscher, P. Weisz and U. Wolff can be thought of as a kind of finger print of a lattice field theory, and it describes the behaviour of an observable, in our case the correlation length, when the lattice size is increased by a factor, in our case we take the factor 1.5 [15]. We build the step-scaling function by calculating the ratios $\xi(L)/L$ and $\xi(1.5L)/\xi(L)$ for each coupling constant and plotting them. The errors are simply derived by Gaussian error propagation. The final step-scaling function is shown in Figure 12. We again observe this behaviour, where increasing the lattice size decreases the correlation length for lower coupling constants.

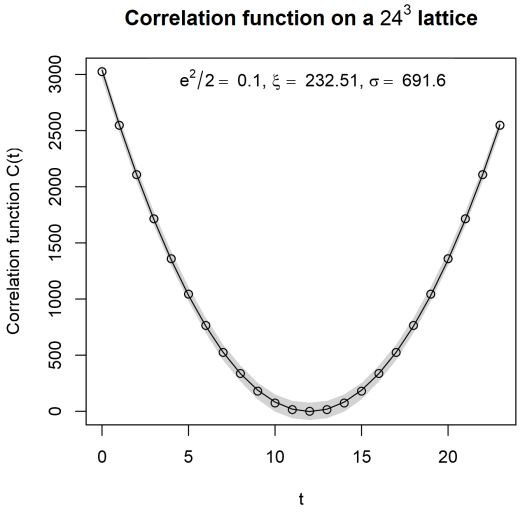

(a) Close to a parabola.

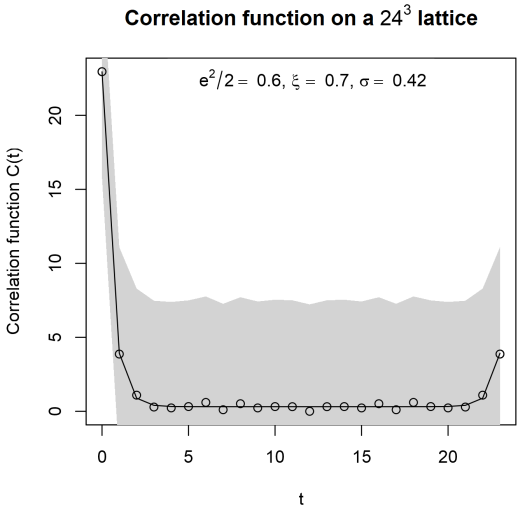

(b) Mostly noise.

Figure 9: Unusable correlation functions.

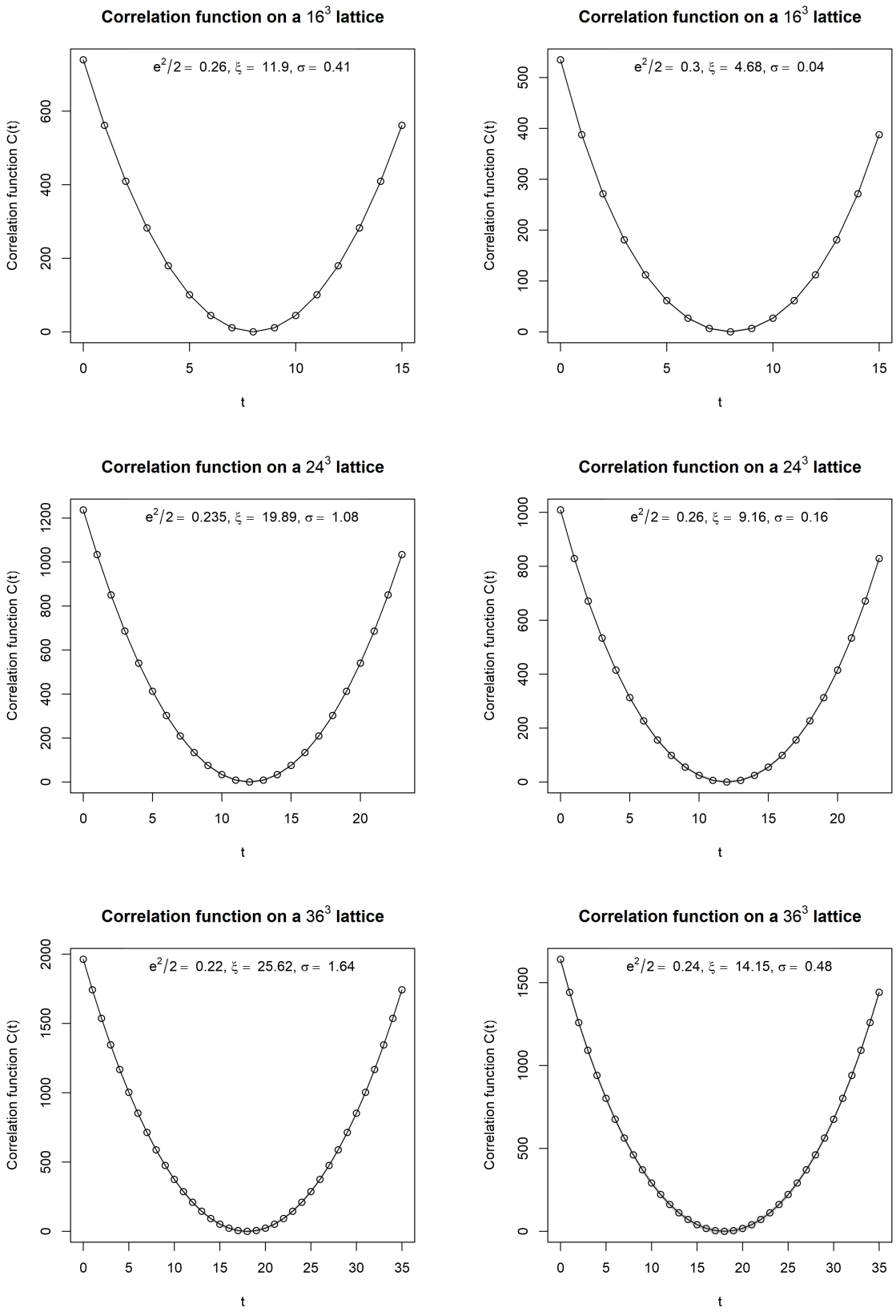

Figure 10: Some correlation functions we used for the correlation length and step-scaling function analysis with a least squares fit line and estimated errors. The values of the coupling constant $e^2/2$, the second moment correlation length ξ and the estimated error σ are given.

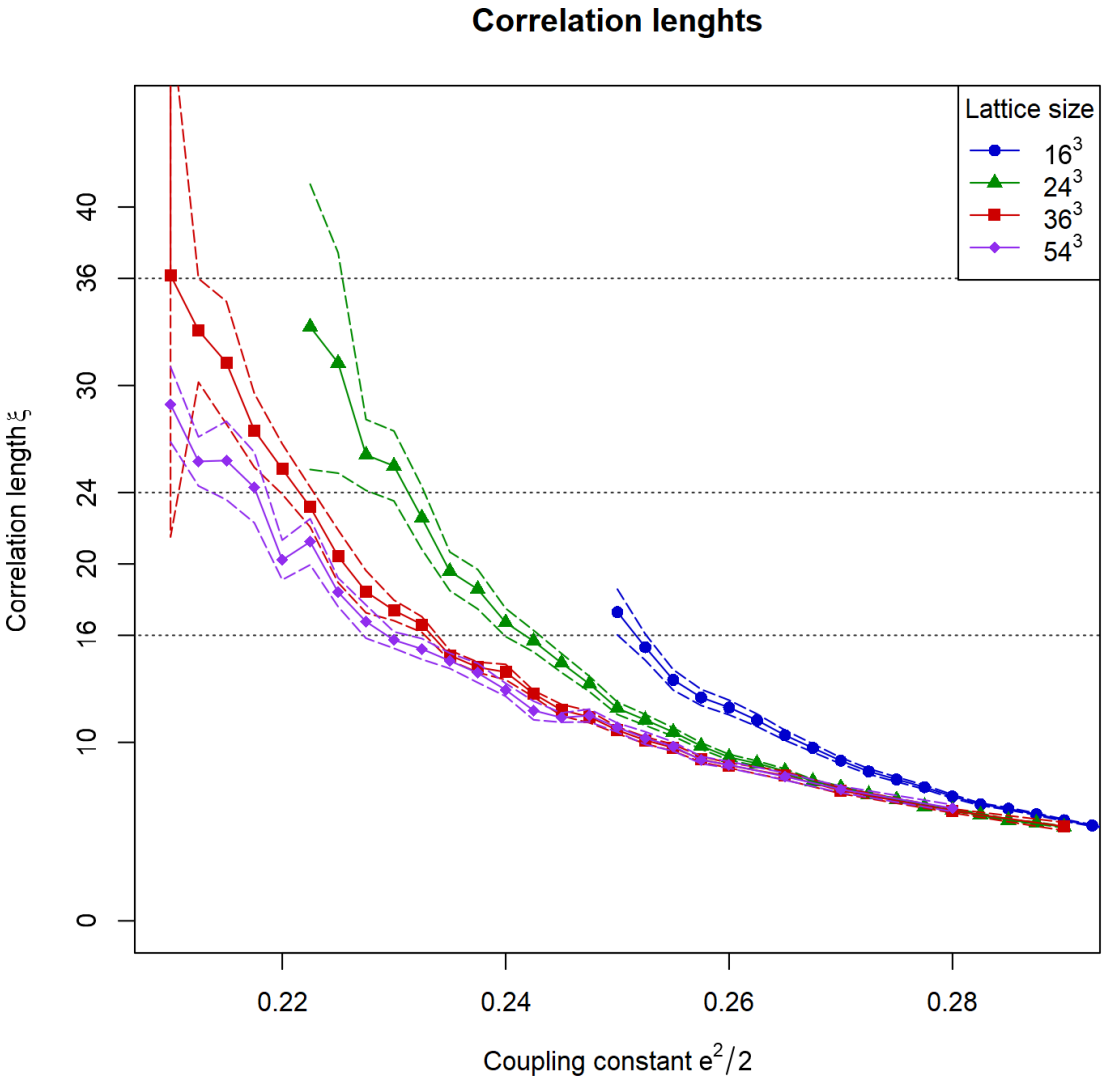

Figure 11: Calculated second moment correlation lengths for different lattice sizes. Here we added a line connecting the data points to guide the eye and the colored dashed lines indicate the standard error.

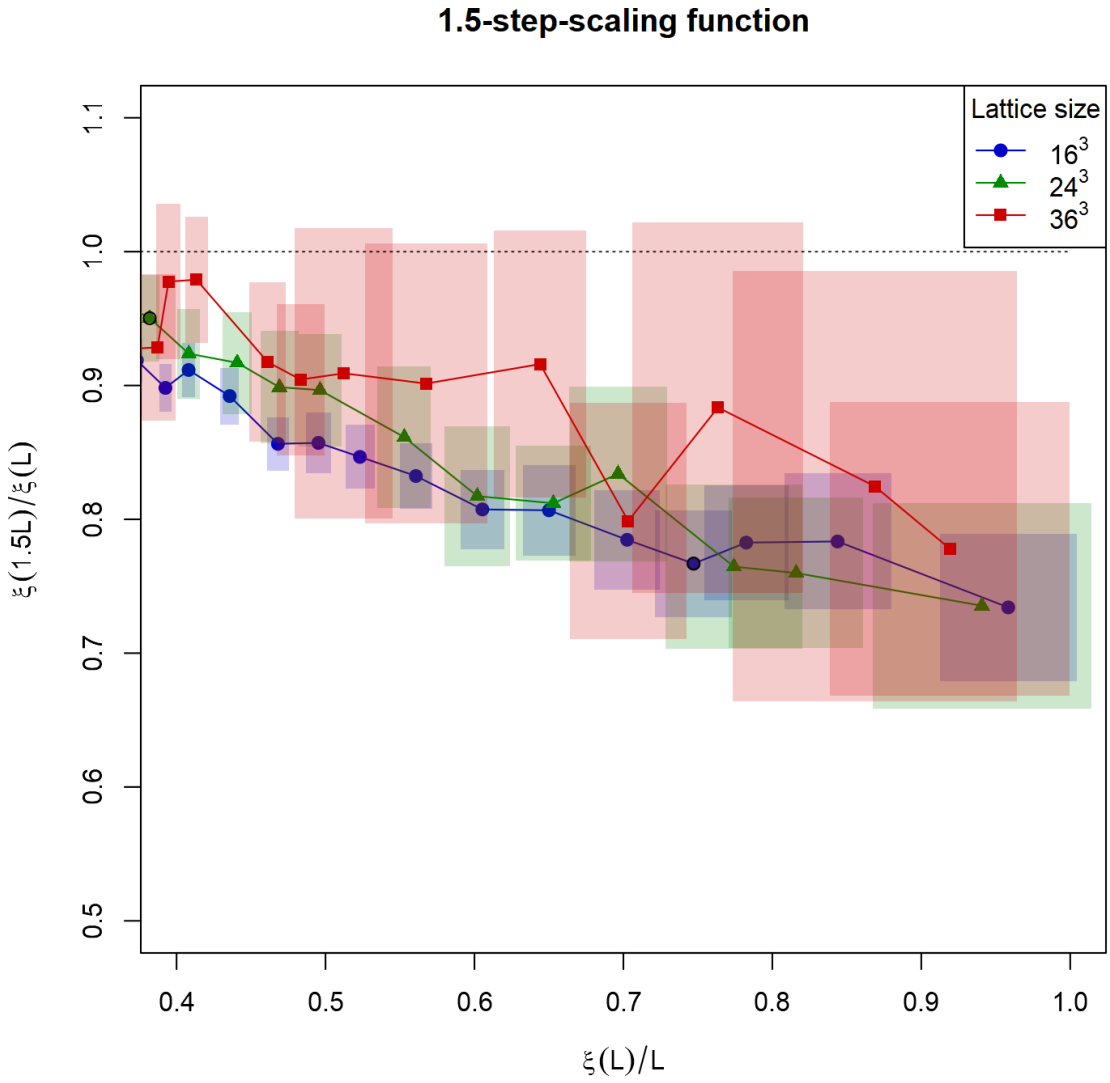

Figure 12: 1.5-step-scaling function from second moment correlation lengths with a line connecting consecutive data points to guide the eye. The boxes indicate the propagated standard error.

Chapter 5

Conclusion

5.1. Summary

Thus we arrive at the conclusion. We were able to derive a formulation of the 3-dimensional U(1) lattice field theory on the dual lattice which allowed us to perform measurements and simulations for both the vacuum case and the case of a particle-antiparticle pair. We developed a Monte Carlo Markov chain lattice simulation and implemented and performed measurements of action, energy, field strength and correlation function observables and estimated their errors. We calculated the string tension for different lattice sizes and coupling constants from the energy observations. We defined a shift-invariant correlation function observable and derived a second moment approach to calculating the correlation length. We compared it to deriving the correlation length via non-linear least squares regression. Finally we calculated the correlation lengths for different lattice sizes and coupling constants and produced a 1.5-step-scaling function.

5.2. Discussion and further proceeding

We now want to pick some of our results and discuss them further. We start at the beginning where we derived the two actions with and without charges. While the action was all we needed in order to start with the lattice simulations, there are more theoretical calculations we omitted here. For one, we omitted calculating the transfer matrix of the system. The transfer matrix would be useful in order to rigorously prove that the surface width observable has the same correlation length dependence as the correlation function, however we consider the discussion in Section 4.1 sufficient for the scope of this thesis.

In Chapter 3 we performed lattice simulations for lattices of sizes 16^3 to 54^3. These were mainly limited by the computation power of the systems we ran them on, and we would have liked to calculate the observables also on a 81^3 lattice, which would have complemented the step-scaling function results nicely. We identified the range for the coupling constants of $e^2/2 \in [0.2, 0.3]$ as our main target by investigating a wide range of coupling constants and inspecting the correlation functions by eye. While this was optimal to find the range to build the step-scaling function, we used the same range to measure the string tension, which in turn makes our string tension result in Figure 8 quite limited in scope. One would have to

perform the same investigation of coupling constants as we have done with the correlation functions for the string tension, however we unfortunately did not have the computing time to do so. Nonetheless we can see that the string tension might approach a continuum limit for increasing lattice sizes.

In Chapter 4, the use of the second moment correlation length allows us to calculate the correlation lengths without relying on non-linear least squares fitting. However we have to note that the choice of what momentum modes to use for the second moment approach is quite arbitrary, as each choice is its own related but different object. We used the first and second momentum mode as it is closest to the original second moment formula, but doesn't utilize the zero mode. We assumed that this would make it less susceptible to higher frequency interference that comes from the correlation function measurement, although we did not test that. It might have been helpful to perform the exact same analysis with the fitting approach as well, in order to compare the two, but our preliminary testing did indicate that the second moment approach was preferable, so we proceeded with it.

As we see in Figure 11, as well as in the step-scaling function in Figure 12, the correlation length observations experience this behaviour where the smaller lattice sizes lead to larger correlation lengths than the larger lattices. This observation is quite astonishing and unexpected. As we were restricted by computing power, we concerned ourselves primarily with the observation of correlation lengths up to the width of the cubic lattice. However, the observation of larger correlation lengths is very much possible, although it yields higher estimated errors. Incorporating data of larger lattices and correlation lengths of smaller lattices, expanding to maybe 1.5 times the lattice width and increasing the statistics are all steps that would be interesting to proceed with.

Bibliography

[1] K. G. Wilson, "Confinement of quarks", Phys. Rev. D **10**, 2445 (1974).

[2] J. Villain, "Theory of one- and two-dimensional magnets with an easy magnetization plane. II. The planar, classical, two-dimensional magnet", J. Phys. France **36**, 581 (1975).

[3] R. V. Gavai, F. Karsch, and H. Satz, "Universality in finite temperature lattice QCD", Nucl. Phys. B **220**, 223 (1983).

[4] M. Göpfert and G. Mack, "Proof of confinement of static quarks in 3-dimensional U(1) lattice gauge theory for all values of the coupling constant", Commun. Math. Phys. **82**, 545 (1982).

[5] N. Manton, "An alternative action for lattice gauge theories", Phys. Lett. B **96**, 328 (1980).

[6] S. Mignani and R. Rosa, "The moving block bootstrap to assess the accuracy of statistical estimates in Ising model simulations", Comput. Phys. Commun. **92**, 203 (1995).

[7] L. Polley and U.-J. Wiese, "Monopole condensate and monopole mass in U(1) lattice gauge theory", Nucl. Phys. B **356**, 629 (1991).

[8] A. M. Polyakov, "Particle Spectrum in Quantum Field Theory", JETP Lett. **20**, 194 (1974).

[9] D. J. Griffiths and D. F. Schroeter, *Introduction to Quantum Mechanics*, 3rd edition (Cambridge University Press, 2018).

[10] H. R. Künsch, "The Jackknife and the Bootstrap for General Stationary Observations", Ann. Stat. **17**, 1217 (1989).

[11] S. Necco, "The static quark potential and scaling behavior of SU(3) lattice Yang-Mills theory", PhD thesis (Humboldt–Universität zu Berlin, 2003).

[12] M. Lüscher, K. Symanzik, and P. Weisz, "Anomalies of the free loop wave equation in the WKB approximation", Nucl. Phys. B **173**, 365 (1980).

[13] H. G. Evertz, M. Hasenbusch, M. Marcu, K. Pinn, and S. Solomon, "Stochastic cluster algorithms for discrete gaussian (SOS) models", Phys. Lett. B **254**, 185 (1991).

[14] A. D. Sokal, *Monte Carlo methods in statistical mechanics: foundations and new algorithms*, Cours de Troisième Cycle de la Physique en Suisse Romande (Lausanne, 1989).

[15] M. Lüscher, P. Weisz, and U. Wolff, "A numerical method to compute the running coupling in asymptotically free theories", Nucl. Phys. B **359**, 221 (1991).

Erklärung

gemäss Art. 30 RSL Phil.-nat. 18

Name/Vorname: Albrecht, Immanuel

Matrikelnummer: 18-109-702

Studiengang: Physics

Bachelor ☐ Master ☑ Dissertation ☐

Titel der Arbeit: Confinement in 3-d U(1) Lattice Gauge Theory

LeiterIn der Arbeit: Prof. Dr. Uwe-Jens Wiese

Ich erkläre hiermit, dass ich diese Arbeit selbständig verfasst und keine anderen als die angegebenen Quellen benutzt habe. Alle Stellen, die wörtlich oder sinngemäss aus Quellen entnommen wurden, habe ich als solche gekennzeichnet. Mir ist bekannt, dass andernfalls der Senat gemäss Artikel 36 Absatz 1 Buchstabe r des Gesetzes vom 5. September 1996 über die Universität zum Entzug des auf Grund dieser Arbeit verliehenen Titels berechtigt ist.
Für die Zwecke der Begutachtung und der Überprüfung der Einhaltung der Selbständigkeitserklärung bzw. der Reglemente betreffend Plagiate erteile ich der Universität Bern das Recht, die dazu erforderlichen Personendaten zu bearbeiten und Nutzungshandlungen vorzunehmen, insbesondere die schriftliche Arbeit zu vervielfältigen und dauerhaft in einer Datenbank zu speichern sowie diese zur Überprüfung von Arbeiten Dritter zu verwenden oder hierzu zur Verfügung zu stellen.

Bern, 20.08.2023

Ort/Datum

Immanuel Albrecht

Unterschrift